Synchronized Relaying in Molecular Communication: An AI-based Approach using a Mobile Testbed Setup

Lisa Y. Debus, *Student Member, IEEE*, Pit Hofmann, *Graduate Student Member, IEEE*, Jorge Torres Gómez, *Senior Member, IEEE*, Frank H.P. Fitzek, *Senior Member, IEEE*, and Falko Dressler, *Fellow, IEEE*

***Abstract*—Relay mechanisms are an important part of communication systems and, therefore, naturally occurring molecular communication (MC) links. Multiple techniques have been proposed for designing MC relay-aided setups, assuming synchronous operation and perfect timing during the decoding process. In this paper, we propose using a reinforcement learning (RL)-based synchronizer to continually adapt a decoding threshold and detect transmitted synchronization frames in a dynamic MC environment. We implement our approach in a two-hop MC link model with mobility and show its advantages compared to filter-based maximum likelihood (ML) synchronization. Thereby, we utilized a macroscale, air-based MC testbed for the experimental determination of the channel impulse response (CIR) for a more realistic channel model. Our simulation results exhibit the potential of an RL-based synchronizer with a similarly high detection rate, a false positive rate one order of magnitude lower, and a misalignment several bit times lower compared to the state of the art.**

***Index Terms*—Molecular Communications, Air-based Communication, Testbeds, Reinforcement Learning, Synchronization**

I. Introduction

Relay mechanisms are naturally conveyed in molecular communication (MC) links as part of biochemical processes. For instance, the insulin secretion of artificial beta cells can be modeled as an amplify and forward (AF) relay mechanism [1]. A similar model is derived for spreading viral infection processes, where infected subjects are studied as store-and-forward relays in [2]. For the purpose of communications, the main motivation to encompass relay-aided setups with two hops [3], [4] or multiple ones [5] is to extend the limited communication range of MC networks. Reporting amplify-and-forward and decode-and-forward mechanisms, research studies evaluate the optimal location of nodes and decision thresholds in fluid mediums [6], as well as the optimal number of relay nodes to minimize communication delay in bacteria colony setups [7]. In the more realistic case of mobile scenarios, theoretical formulations for the detection threshold and symbol error rate probability are derived for one hop [8] and multiple hops [9], where the two communication nodes and the relay node follow a Brownian motion pattern. In vessel-like scenarios, the optimal threshold and amount of released molecules are also evaluated for multiple-hop links, like in [10], [11].

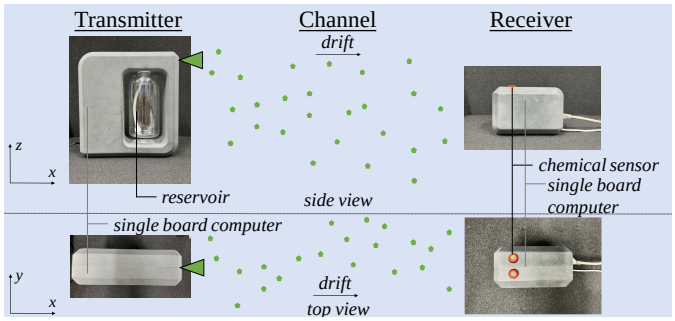

Fig. 1. Air-based macroscale molecular SISO communication testbed, cf. [15]; first presented in [16]. The green triangle denotes the propulsive release mechanism of the molecules [17].

However, previous works assume that nodes operate synchronously and information is decoded with perfect timing. In practice, receivers require a synchronization mechanism with the symbol time, enabling data decoding. Otherwise, the impact of symbol time offset (STO) will degrade the communication performance, preventing data transmission. Prior research contends the conception of symbol time synchronizers in MC links using a maximum likelihood approach [12], [13]. Yet, synchronization mechanisms in MC relay-aided links, including the mobility of nodes, are missing.

Extending our previous work in [14], we investigate a reinforcement learning (RL) method to realize synchronization in a two-hop link. We are mainly driven by the flexibility of machine learning models, which allows us to deal with the uncertainty of mobility and threshold detection levels for incoming symbols. We realized two agents to enable synchronization in the relay node, operating as decode-and-forward, and on the final destination mobile node. Accounting for a realistic setup, we perform the training using data from the air-based testbed illustrated in Fig. 1. We use this point-to-point testbed to emulate a two-hop link with mobility on the receiver side in the form of Brownian motion. Results indicate the superiority of the two agents' threshold adaption process, overestimating the end-to-end channel model and transmission parameters, as in the case of maximum likelihood formulations.

Lisa Y. Debus, Jorge Torres Gómez, and Falko Dressler are with the School for Electrical Engineering and Computer Science, TU Berlin, Berlin, Germany, email: {debus, torres-gomez, dressler}@ccs-labs.org.

Pit Hofmann and Frank H.P. Fitzek are with the Deutsche Telekom Chair of Communication Networks, Technische Universität Dresden, Dresden, Germany; F. Fitzek is also with the Centre for Tactile Internet with Human-in-the-Loop (CeTI), Dresden, Germany, email: {pit.hofmann, frank.fitzek}@tu-dresden.de.

This work was supported in part by the project IoBNT funded by the German Federal Ministry of Education and Research (BMBF) under grant numbers 16KIS1986K & 16KIS1994 and by the project NaBoCom funded by the German Research Foundation (DFG) under grant number DR 639/21-2. This work was also supported by DFG as part of Germany's Excellence Strategy—EXC 2050/1—Cluster of Excellence "Centre for Tactile Internet with Human-in-the-Loop" (CeTI) of Technische Universität Dresden under project ID 390696704 and BMBF in the program of "Souverän. Digital. Vernetzt." Joint project 6G-life, grant number 16KISK001K.

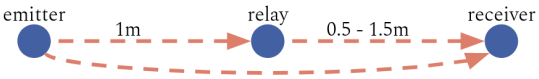

Fig. 2. Mobility model. The emitter and relay remain static while the receiver moves within a given range. This mobility results in a change of CIR.

II. System Model

As the system model, we address a relay-aided link as a two-hop connection. We assume static relay and emitter nodes and the receiver node moving randomly according to Brownian motion. This scenario occurs in monitoring applications where a mobile fusion node collects data from a static sensor node. Addressing realistic channels, we use measurements from the air-based macroscale testbed in Fig. 1 to implement a more realistic end-to-end channel.

A. Macroscale MC Testbed

For the experimental determination of the channel impulse response (CIR) we utilize the macroscale SISO MC testbed, see Fig. 1, as initially presented in our earlier work [15]. All components in the experimental setup are commercially available off-the-shelf products. Specifically, an atomizer functions as the propulsive release mechanism of the molecules [17], and the MQ-3 gas sensor serves as the chemical sensor at the receiver side. Two Raspberry Pi single-board computers are utilized for electronic control of the mechanical release mechanism and the transmission of the electrical signal from the chemical sensor to a local PC for post-processing. The transmitter comprises a sprayer for the mechanical release of the molecules, here ethanol molecules, and a reservoir for the molecules. The reservoir contains an ethanol solution diluted in a mass ratio 1/4, i.e., four parts distilled water and one part 99.99 % ethanol by mass. As the modulation technique, we use on-off keying (OOK). The activation of the mechanical release of the molecules, representing a `1`, releases approximately 1.5 g diluted ethanol [15], which corresponds to a total number of 3.92×10^{21} released molecules, while a `0` signifies no emissions. The propagation of the molecules from the transmitter to the receiver is supported by an additional drift of average speed $v = 3{:}5\,\mathrm{m/s}$.[1] The receiver incorporates an electrochemical sensor that measures the concentration level of the molecules with a sampling frequency of 5 Hz. Using the described setup, we collect measurements and approximate the testbed's CIR as described in Section II-B2 to be used in the simulated relayed communication system. The experimental setup consists of a transmitter and a receiver, following Fig. 1. The relay only exists in the simulation model. The reception and relay process for the simulation model follows Section II-B3.

B. Mobile Communication Model

We emulate a mobile communication link by evaluating the CIR in a time-space grid. The number of received molecules is computed by reading the CIR in the corresponding time-space coordinates following the time-varying receiver's position. We devise the following components to carry out this calculation and model a mobile communication link.

[1]An anemometer *Airflow Instruments LCA301* was used for measuring the velocity of the airflow.

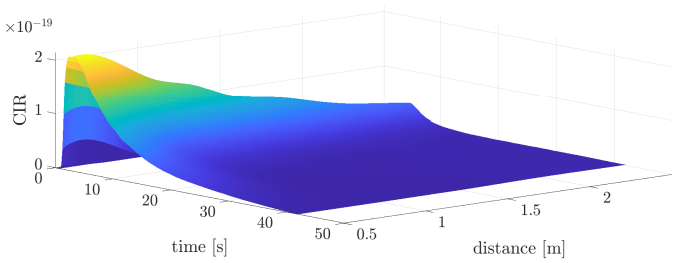

Fig. 3. Average CIR of the testbed created by interpolating the recorded measurements.

1) Receiver Mobility: We simulate 1D mobility for the receiver according to Brownian motion. We define the receiver's diffusion coefficient with D_{Rx}, which also provides the distance it can move within a given time step t as $= \sqrt{2D_{\mathrm{Rx}}\ t}$ [18]. The receiver moves by after every 5 bits. It can therefore receive a full synchronization frame if one was transmitted without moving during its transmission. It can move within a distance range of 0.5 m to 1.5 m from the relay. All communication participants are aligned along the direction of their sprayer. A schematic of the approach is shown in Fig. 2.

2) Spatio-Temporal Channel Impulse Response: We render a spatio-temporal surface for the CIR using the testbed measurements for the total number of received molecules as represented in Fig. 3. To compute this surface, we collect sequences with testbed measurements for distances between $0{:}5\,\mathrm{m}$ and $2{:}5\,\mathrm{m}$ in steps of $0{:}25\,\mathrm{m}$ and normalize these sequences with the total number of released molecules. We later interpolate these sequences to approximate the CIR for the distances between the recorded steps.[2] For each transmitter-receiver-distance in the testbed setup between $0{:}5\,\mathrm{m}$ and $2{:}5\,\mathrm{m}$, we measure the alcohol concentration at the receiver side over 40 s with a sampling frequency of 5 Hz. A total number of ten measurements is considered per distance and the average is calculated over all measurements per distance. The averaged values are interpolated using the spline interpolation `interp2` provided in Matlab with a grid relating its step size to the minimum step width possible to be taken by the receiver, i.e., as given by . Fig. 3 shows the resulting surface of the CIR for a distance of $0{:}5$ to $2{:}5\,\mathrm{m}$ and a time interval of 0 to $40\,\mathrm{s}$. In the simulation, we add Poisson noise to our CIR [19]. The resulting signal has a signal to noise ratio (SNR) of 30 dB.

3) Reception and Relay Process: We calculate the number of expected molecules at the relay and receiver node with the CIR-surface in Fig. 3 after scaling it with the total number of released molecules. The relay node uses a decode-and-forward strategy, aiming to deploy the same receiver structure at the relay and receiver nodes. The relay node uses the same detector and synchronizer as the receiver. Frames are detected and forwarded to the receiver, irrespective of their correctness. Furthermore, at the relay node, we consider only the molecules released by the emitter, and at the receiver node, we superpose the emitter and the relay emissions. We also include the retransmission delay produced by the decode-and-

[2]The minimum distance of $0{:}5\,\mathrm{m}$ is due to the propulsive release of the molecules influencing the achievable communication range within the testbed.

forward mechanism at the relay node. To compute the number of received molecules, we sample the CIR-surface in Fig. 3 with the actual distance to the emitter over time. Each time the receiver changes its position, we evaluate the distance to the emitter and relay in the simulation and read the sample on the CIR surface accordingly.

We use the same CIR-surface on both the relay and the receiver side. This means that the relay node placed between the transmitter and the receiver is considered transparent in the transmission between these two nodes. In practice, placing the relay node between the transmitter and the receiver would reduce the number of molecules reaching the receiver side, as most of them would already be received by the relay. The relay's inclusion in the CIR of the receiver node would, therefore, reduce the interference produced by the transmitter's original transmission on the transmission from the relay to the receiver node. We assume that the reduction of interference would likely improve the transmission quality from the relay to the receiver. In our simulation, we assume the worst case scenario by evaluating the maximum possible interference with the relay node acting as a transparent receiver.

III. RL-BASED SYNCHRONIZER

We realize an RL-based synchronizer for the described relayed MC system in a Matlab/Simulink environment. Fig. 4 depicts the block diagram for the synchronizer. The modeling of the channel, including node mobility, is implemented with three blocks, in which the receiver position is evaluated, the CIR is sampled, and the expected number of molecules based on the transmitted frame sequence is calculated. The synchronizer is made up of a threshold detector and a correlator block. The threshold detector uses the threshold to decode the expected number of molecules m_{rx} at sample time x into a 0, i.e., $> m_{\mathrm{rx}}$, or a 1, i.e., m_{rx}. The correlator compares the decoded bit sequence with the expected synchronization bit sequence according to the state diagram shown in Fig. 5 and outputs the resulting synchronization clock if a synchronization frame is detected. Additionally, the sample time offset shifter block shifts the sampling time offset to the maximum of the first bit in the detected synchronization frame. The RL agent is integrated with the threshold decoder. Based on observations of the current number of molecules and threshold and a reward evaluating its ongoing performance, the RL agent continuously adapts the used threshold . In the following, we explain the structure of the RL loop and the implemented RL agents with their training process.

A. Reinforcement Learning-Loop

The RL-loop used to train the adaptive threshold setting is based on three values: observations, reward, and actions. The observations must represent the system's current state to the RL agent. In the presented approach, we use

$$\text{observation} = m_i \quad _i \tag{1}$$

to define the observation, where m_i denotes the number of observed molecules and $_i$ is the detection threshold at the current sampling time i. In our system, we expect a spike in

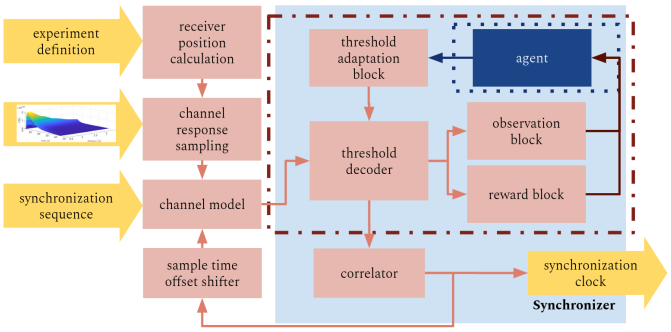

Fig. 4. Block diagram of the RL-based synchronizer performing threshold setting in a relayed setup in the presented testbed.

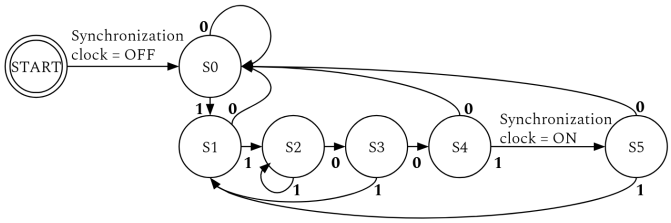

Fig. 5. State diagram of the RL-based synchronizer's correlator. By moving through the states according to the decoded bit value, the correlator detects synchronization frames at state S5.

the number of molecules to occur for the transmission of a 1 and not for the transmission of a 0. With the threshold $_i$ set correctly to decode both possible bit values, the observed difference is negative for the transmission of a 0 and positive for the transmission of a 1. The given value, therefore, enables the agent to deduct the last transmission and use this knowledge to adapt the next threshold $_{i+1}$ to the state of the system.

The agent is rewarded for the system's current state at the end of each run through the RL-loop. As the current state results from the agent's last action, it implicitly judges the agent's performance. We base our reward

$$\text{reward} = 0 \quad (m_i \quad _i)^2 \quad \frac{1}{c} \tag{2}$$

on a quadratic cost for the difference between the number of molecules m_i and the threshold $_i$ at the current sampling time i. The reward is scaled with factor c. The farther the threshold from the number of molecules at time i, the higher the cost for the agent's action. As the agent strives to minimize the cost in the long term, it reduces the distance between the threshold and number of molecules for transmitted 0s and 1s. During the training, the value of the next transmitted bit is chosen at random, and the RL agent must develop a threshold adaption strategy that will minimize the cost produced by the distance in case of both possible bit values.

Over time, this reward formulation pushes the agent to maximize the noise margin between the possible transmission of a 0 and a 1 by setting the threshold to the expected minimum cost, which is in the middle of the two possible molecule levels. This minimum cost and, therefore, maximum reward is visualized in Fig. 6. The reward scaling factor c is tuned for the RL agent during its hyper-parameter tuning. In our system, the tuned value for c is 1000.

Based on the observations and the reward, the agent adapts the current threshold by passing the action $_{th}$ to the

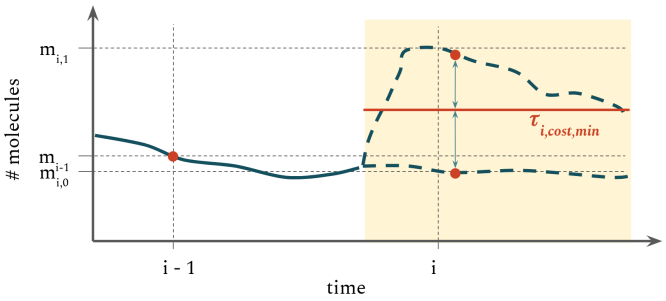

Fig. 6. The RL agent's reward maximizes the noise margin between the potentially received number of molecules in case of a 1 or a 0. The sampling interval between point i and $i-1$ equals the bit time.

environment. The value $_{th}$ is added to the current threshold , and the result is used in the next loop. The range of possible action values must be high enough to enable accurate threshold adaption while still enabling efficient learning.

B. Implementation and Training of the RL Agents

We implement the presented RL approach using a proximal policy optimization (PPO) agent each for the relay and the receiver node. The two agents include a long short-term memory (LSTM) layer to facilitate the continuous adaption of the threshold, and their hyperparameters are tuned separately.

As the performance of the receiver node relies on the forwarding performed by the relay node, we train the relay node first. For the training process, 375 000 random bits are transmitted at the distance of 1 m. Following its successful training, we deploy the relay node RL agent for the training process of the second agent. The RL agent at the receiver node is trained for 375 000 random bits at a distance varying from 0:5 to 1:5 m. For both agents, we experimentally evaluated longer training times and found that training times longer than 375 000 bits lead to no further detectable improvements in the agents' performance.

IV. Results

We evaluate the performance of the RL-based synchronizer regarding the true positive rate (TPR) and false positive rate (FPR) of its frame detection capabilities and the achieved STO. As a baseline, we use the filter-based maximum likelihood synchronizer at the relay and receiver nodes [12, Eqs. (7) and (8)]. Similar to the RL implementation, the relay node in the filter-based approach retransmits the synchronization frame in case of detection; otherwise, it transmits an empty frame. The detection threshold of the filter-based ML estimator was adapted by hand by minimizing the overall frame error rate (FER). We comparatively illustrate results for the filter-based synchronizer and RL mechanisms with the TPR and FPR for the detection of synchronization frames, and the STO.

A. Evaluation Setup

We simulate 10^5 frame transmissions in total, of which half are synchronization frames with the bit sequence [11001] and the other half are frames with random bit sequences. The bit rate during the evaluation is 0:25 Hz. The distance between the emitter and the relay node is static at 1 m. In contrast, the distance between the relay and the receiver starts at 1 m and changes according to a receiver diffusion coefficient of $D_{\mathrm{Tx}} = 8{:}4 \quad 10^{-5}\,\mathrm{m}^2/\mathrm{s}$. The total number of evaluated frames is split into 100 evaluation runs consisting of 1000 frames each. In each evaluation run, the receiver moves randomly in 1D based on D_{Tx}.

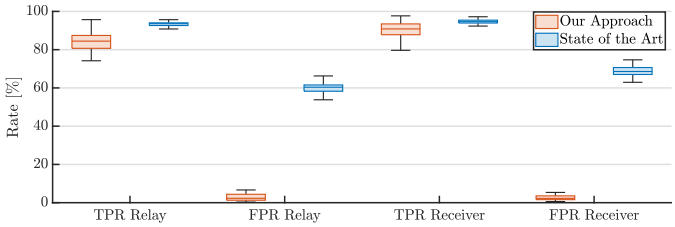

Fig. 7. Detection rates at the relay and receiver nodes: TPR and FPR of the synchronization frames for the filter-based ML and RL synchronizers.

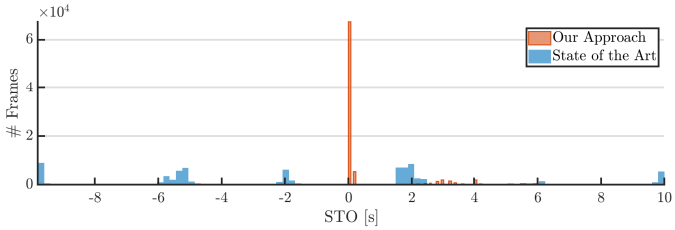

Fig. 8. Symbol time offset at the receiver node: STO of the detected synchronization frames of the filter-based ML and RL approach.

B. Misdetection Rate

To evaluate the detection performance of our approach, we evaluate the TPR, i.e., the detection rate if a synchronization frame was sent, and the FPR, i.e., the misdetection rate if no synchronization frame was sent. The results at the relay and the receiver node for the filter-based ML and the RL-based synchronizers are shown in Fig. 7.

Both approaches achieve TPR values of 80% or higher at both nodes. The filter-based ML synchronizer generally detects slightly more synchronization frames correctly. While both approaches correctly detect approximately the same amount of synchronization frames, their FPRs are very different. The RL agent always achieves an FPR below 5%. The filter-based ML approach, on the other hand, regularly has an FPR of more than 50% at the relay node and more than 65% at the receiver node.

The difference in the performance can be explained by the different concepts of the two approaches. The RL agent looks at each bit separately and rarely detects a whole synchronization frame where none was sent. On the other hand, the filter-based approach uses a simple threshold to define the synchronizer's sensitivity for the whole frame. With a sensitivity set high enough to detect enough synchronization frames, the FPR increases. The difference in the FPR shows the better adaptability and accuracy of the RL approach in high inter-symbol interference dynamic surroundings.

C. Symbol Time Offset

Fig. 8 shows the STO of the correctly detected synchronization frames for the evaluated RL and filter-based ML approach. The results clearly show the better adaptability of the presented

RL approach to the simulated system. While the filter-based ML approach only considers full frames and regularly ends up with several bit times STO, the RL-based synchronizer achieves an STO much nearer to the actual start time of the synchronization frame. The agent works on a bit-by-bit basis and, as it must detect the first bit correctly to detect the whole frame correctly, it keeps the STO at under 4 s and in most cases, even at under half a bit time.

D. Further Discussion

The presented results show that the relayed setup from transmitter via relay to receiver node does not significantly impact the detection rates compared to the direct transmission between the transmitter and the relay node. We only observe slight changes in the performance between the receiver and the relay node for both synchronization approaches. The TPR rises slightly for the RL-based synchronizer, and the FPR rate rises by a few percent for the filter-based maximum likelihood synchronizer as shown in Fig. 7. Overall, these changes are minor, though, and we do not observe a big difference in the results. The relay node, which receives only one transmission at a static distance, and the receiver node, which receives the transmissions from the transmitter and the relay node at changing distances, perform similarly.

While our results show a first step towards intelligent synchronization in dynamic MC systems, our approach does not perform well enough to use it for combined synchronization and decoding. With a median bit error rate (BER) of 9%, the RL agent is not yet reliable enough. The performance of the RL-based synchronizer could be improved by employing the following measures. Currently, only one observation is used. This offers the agent a very limited view of the current environment state. Including additional values, e.g., threshold $_i$ or minimum and maximum value over the last sampling interval, could improve the threshold adaptation's accuracy. The extended description of the environment state could particularly improve the agent's performance for CIR cases in which the distinction between a transmitted `0` and a transmitted `1` becomes more complicated. Additionally, the shifting of the sampling offset could be added to the agent's actions space. This would enable the agent to adapt its sampling offset to the point where the best distinction between the transmitted symbols is possible.

In addition to changes to the RL agent's setup that could improve its performance, we plan to explore more complex setups in our future work. We will extend the given setup to multi-link scenarios, including multiple transmitters and relays. Regarding the movement, we will explore the cases with the receiver moving nearer to the relay than 0.5 m.

V. Conclusion

This work shows the immense potential of RL-based threshold adaption in a relay-based MC system with mobility. After training, our approach exhibits a high TPR of the sent synchronization frames while at the same time keeping the FPR and STO low. In future work, we intend to extend our approach to more robust system models and implement it directly in the testbed.

References

[1] T. M. Theodoridis, S. A. Tegos, P. D. Diamantoulakis, V. Jamali, and G. K. Karagiannidis, "Glucose Regulation Through Cooperative Molecular Communication," *IEEE Communications Letters*, vol. 27, no. 11, pp. 2933–2937, Nov. 2023.

[2] M. Schurwanz, P. A. Hoeher, S. Bhattacharjee, M. Damrath, L. Stratmann, and F. Dressler, "Infectious Disease Transmission via Aerosol Propagation from a Molecular Communication Perspective: Shannon Meets Coronavirus," *IEEE Communications Magazine, Special Issue on Nano-Networking for Nano-, Micro- and Macro-Scale Applications*, vol. 59, no. 5, pp. 40–46, May 2021.

[3] J. Angjo, A. E. Pusane, H. B. Yilmaz, E. Basar, and T. Tugcu, "Asymmetrical Relaying in Molecular Communications," *IEEE Transactions on NanoBioscience*, vol. 21, no. 4, pp. 570–574, Oct. 2022.

[4] B. Atakan and O. B. Akan, "On Molecular Multiple-Access, Broadcast, and Relay Channel in Nanonetworks," in *ACM/ICST BIONETICS 2008*, Hyogo, Japan: ICST, Nov. 2008.

[5] J. Kirchner, "Quick Macroscopic Diffusion-Based Molecular Communication With Wavelike Propagation by Use of a Suspension of Relay Cells," *IEEE Communications Letters*, vol. 27, no. 4, pp. 1125–1129, Apr. 2023.

[6] Z. Cheng, J. Yan, J. Sun, Y. Tu, and K. Chi, "Joint Optimizations of Relays Locations and Decision Threshold for Multi-Hop Diffusive Mobile Molecular Communication With Drift," *IEEE Transactions on NanoBioscience*, vol. 21, no. 3, pp. 454–465, Jul. 2022.

[7] M. C. Gursoy, S. Gupta, O. S. Venturelli, and U. Mitra, "Optimizing the Spatial Topology of Bacterial Relay Systems: Delay Minimization," in *IEEE ICC 2022*, Seoul, South Korea: IEEE, May 2022.

[8] Z. Cheng, J. Yan, Y. Tu, K. Chi, and M. Xia, "Mobile Two-Way Molecular Communication via Diffusion Using Amplify-and-Forward and Analog Network Coding," *IEEE Transactions on NanoBioscience*, vol. 21, no. 2, pp. 273–285, Apr. 2022.

[9] Z. Cheng, Y. Tu, J. Yan, and Y. Lei, "Amplify-and-forward relaying in mobile multi-hop molecular communication via diffusion," *Elsevier Nano Communication Networks*, vol. 30, p. 100 375, Dec. 2021.

[10] L. Chouhan, P. K. Sharma, and N. Varshney, "Optimal Transmitted Molecules and Decision Threshold for Drift-Induced Diffusive Molecular Channel With Mobile Nanomachines," *IEEE Transactions on NanoBioscience*, vol. 18, no. 4, pp. 651–660, Oct. 2019.

[11] N. Varshney, A. Patel, J. Haselmayr, A. K. Jagannatham, P. K. Varshney, and A. Nallanathan, "Impact of Intermediate Nanomachines in Multiple Cooperative Nanomachine-Assisted Diffusion Advection Mobile Molecular Communication," *IEEE Transactions on Communications*, vol. 67, no. 7, pp. 4856–4871, Jul. 2019.

[12] V. Jamali, A. Ahmadzadeh, and R. Schober, "Symbol Synchronization for Diffusion-Based Molecular Communications," *IEEE Transactions on NanoBioscience*, vol. 16, no. 8, pp. 873–887, Dec. 2017.

[13] A. Noel and A. W. Eckford, "Asynchronous peak detection for demodulation in molecular communication," in *IEEE ICC 2017*, Paris, France: IEEE, May 2017.

[14] L. Y. Debus, P. Hofmann, J. Torres Gómez, F. H. P. Fitzek, and F. Dressler, "Reinforcement Learning-based Receiver for Molecular Communication with Mobility," in *IEEE GLOBECOM 2023*, Kuala Lumpur, Malaysia: IEEE, Dec. 2023, pp. 558–564.

[15] P. Hofmann, J. Torres Gómez, F. Dressler, and F. H. P. Fitzek, "Testbed-based Receiver Optimization for SISO Molecular Communication Channels," in *IEEE BalkanCom 2022*, Sarajevo, Bosnia and Herzegovina: IEEE, Aug. 2022, pp. 120–125.

[16] N. Farsad, W. Guo, and A. W. Eckford, "Tabletop Molecular Communication: Text Messages through Chemical Signals," *PLOS ONE*, vol. 8, no. 12, pp. 1–13, Dec. 2013.

[17] S. Lotter, L. Brand, V. Jamali, M. Schäfer, H. M. Loos, H. Unterweger, S. Greiner, J. Kirchner, C. Alexiou, D. Drummer, G. Fischer, A. Buettner, and R. Schober, "Experimental Research in Synthetic Molecular Communications – Part II," *IEEE Nanotechnology Magazine*, vol. 17, no. 3, pp. 54–65, Jun. 2023.

[18] V. Jamali, A. Ahmadzadeh, W. Wicke, A. Noel, and R. Schober, "Channel Modeling for Diffusive Molecular Communication - A Tutorial Review," *Proceedings of the IEEE*, vol. 107, no. 7, pp. 1256–1301, Jul. 2019.

[19] A. Noel, K. Cheung, and R. Schober, "A Unifying Model for External Noise Sources and ISI in Diffusive Molecular Communication," *IEEE Journal on Selected Areas in Communications*, vol. 32, no. 12, pp. 2330–2343, Dec. 2014.